THE JOURNAL OF PHYSICAL CHEMISTRY C
A JOURNAL OF THE AMERICAN CHEMICAL SOCIETY

pubs.acs.org/JPCC

Article

How Crystallization Affects the Oriented Attachment of Silver Nanocrystals

Giovani M. Faccin,* Zenner S. Pereira, and E. Z. da Silva

Cite This: *J. Phys. Chem. C* 2021, 125, 6812–6820

Read Online

ACCESS | Metrics & More | Article Recommendations | Supporting Information

ABSTRACT: Oriented attachment processes between nanocrystals provide a promising route for the synthesis of mesocrystals that, although made of the same elements as their usual crystal counterparts, nevertheless possess very distinct physical and chemical properties that can be explored for technological applications. In this study, the oriented attachment process experimentally observed between silver nanocrystals is analyzed through a systematic approach involving a series of molecular dynamics simulations. The simulations elucidate how the crystallization process between silver nanocrystals leads to either imperfect oriented attachment or perfect oriented attachment, how likely those processes are to occur and how faceting affects their outcome. This information can be explored to develop new strategies aimed at triggering specific crystallization processes that take place during mesocrystal growth, thus allowing control over the characteristics of the final synthesized material.

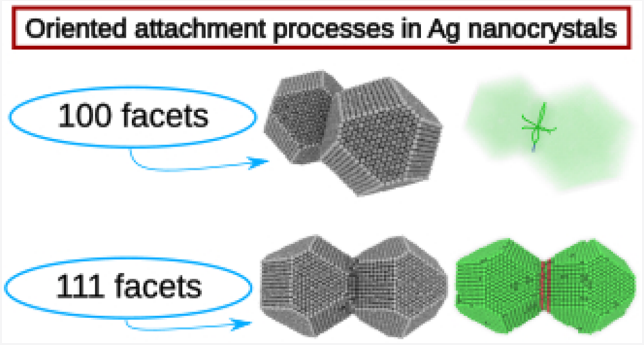

INTRODUCTION

Conventional particle sintering,[1] in it is simplest form, is straightforward: it consists of pressure and temperature applied to powders in order to shape them into a solid. However, without control, this leads to formation of random, multigrain structures. Higher control of the sintering process is desirable, and one path toward it is to employ bottom-up synthesis approaches that explore interactions between nanocrystals (NCs) and an external element. This can lead to attachments between specific NC facets becoming more viable and/or growth accelerating in specific crystallographic directions, allowing, for example, anisotropic crystal growth.[2] Examples of external elements explored in the literature include the effect of surfactants[3] in wet chemistry synthesis, NC interactions mediated by light,[4] magnetic fields,[5] and electron beams.[6−8]

In classical crystal growth, supersaturated solutions nucleate primary, tiny clusters. From these, larger spheroid nanoparticles (NPs) grow by precipitation of mass from the environment, at the expense of dissolved ions and the dissolution of smaller NPs from the environment, in a process known as Ostwald ripening (OR). This effect also mediates island growth in thin film surfaces, as studied, for example, for Ag[9] some time ago. As the NP grows, surface energy anisotropy and surface diffusion then leads to the formation of NCs that obey Wulff-shaped formulations.[10]

However, classical crystallization alone is not expected to be enough to obtain nanostructured mesocrystals,[11] which pose an interesting frontier in materials science. At some point, a flavor of nonclassical pathways involving oriented attachment (OA) that can manifest itself in variants such as perfect oriented attachment (POA), imperfect oriented attachment (IOA), and/or random agglomeration (RA)[2] has to occur, in order to produce dimers, trimers, and more complex structures from primary, NP building blocks. Bahrig et al.[12] postulated two main principles for OA: (i) fusion between NPs in colloidal solutions, through effective collisions that result in irreversible OA, which in turn require crystal alignment between NPs *prior* to the collision and (ii) coalescence induced by particle rotation (CIPR), in which attractive forces between NPs are greater than repulsive forces, thus allowing NPs to touch and interact, forming an interface, the dynamics of which will dictate the remaining OA process. Zhang et al.[13] further added progress on understanding OA phenomena by discussing the role of electrostatic fields originating in the periodicity of crystal structures that surround attaching NPs and how their interactions contribute to generating forces that affect NP OA. They also discuss the role of solvent-surface interactions as a factor that affects the strength of attraction and barrier for attachment. These effects are illustrated, for example, in the work of Balankura et al.[14] who have shown that

Received: November 16, 2020
Revised: February 27, 2021
Published: March 11, 2021

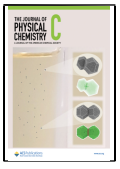

Downloaded via UNIV ESTADUAL DE CAMPINAS on April 1, 2021 at 10:27:30 (UTC).
See https://pubs.acs.org/sharingguidelines for options on how to legitimately share published articles.

© 2021 American Chemical Society

https://dx.doi.org/10.1021/acs.jpcc.0c10321
J. Phys. Chem. C 2021, 125, 6812–6820

when solvents are considered in OA between Ag nanoplates, they can lead to the prevalence of kinetically favored OA pathways over thermodynamically favored ones.

In this study, we focus on ideas derived from the CIPR concept. However, instead of applying it to nanoclusters or spherical nanoparticles that typically emerge from coalescence events, we've worked with larger, Wulff-shaped nanocrystals, in the solid state. Because of their larger size, Wulff-shaped NCs are able to better preserve their surface crystalline facets, thus avoiding coalescence in favor of sintering in events that involve both POA and IOA. We suppose that an aggregation mechanism was set in place so that primary Wulff-shaped Ag NCs can attach. This implies that our study is focused on what happens after attachment between facet surfaces takes place. Recent studies involving NCs composed of naturally polar materials[15,16] indicate that effective dipole electric fields emanate from them that act to produce torques that align the NCs in solution prior to their attachment. For NCs of conductive elements that do not present natural electric dipoles, attractive and repulsive forces can also be triggered using induction of electric dipoles by the interaction between the NCs and a TEM electron beam.[6,8] However, for the case of pure Ag NCs in solution outside the influence of external electromagnetic fields, such interesting long-range field effects that lead to NC interaction and orientation prior to attachment are not expected. Nevertheless, nanostructures that emerge from OA of pure Ag NCs do exist. Thus, it becomes relevant to study the crystallization dynamics of the system in vacuum, in order to understand how it can lead to observed self-assembled nanostructures. We would like to also point out the solvent effect: if a solvent is present, it can act toward providing kinetic synthesis routes that result in preference for attachment between specific facets, or even no attachment at all. These relations depend on the characteristics of the medium in which OA takes place. However, in our view, before considering this extra layer of complexity to this problem, it would be beneficial to inspect the crystallization dynamics of the system in vacuum, without medium effects (electromagnetic fields, chemical solvents, surfactants), so that in future works the role of different types of medium can be established in contrast to the vacuum reference. In this work, we use Molecular Dynamics (MD) simulations to evaluate the outcomes of attachment events for a variety of initial configurations between Ag NCs, thus mapping the behavior of the crystallization process along it. From this analysis, the role of crystallization during OA and how it leads to POA or to IOA for Ag NCs is obtained.

COMPUTATIONAL METHODS

MD simulations were performed using the LAMMPS package[17−20] and the embedded atom model (EAM)[21−24] with the parametrization for Ag from Sheng et al.[25] The EAM effective potential was designed to provide a description that is the closest to experimental data as possible and was constructed in two steps: the first corresponds to fitting density functional theory (DFT) calculations for a variety of scenarios, while the second corresponds to a refinement in which the potential functions fitted from DFT data are empirically transformed in order to better match experimental data.[25] This results in a Ag effective potential that, while developed from DFT, has some of DFT's intrinsic errors and approximations removed empirically, thus providing excellent description of experimental phenomena.[26]

Canonical ensemble molecular dynamics was simulated through Nosé−Hoover thermostat chains.[27−29] Visualizations were created using the Ovito[30] package, including the common neighbor analysis (CNA) of Dana et al.[30] and the dislocation analysis of Stukowski et al.[31] Additional simulation parameters are available in the Supporting Information.

Prior to the sintering events, the individual NC model was simulated in isolation at 500 K for 20 ns, in order to attain thermal and structural equilibrium. Except for small thermal agitation and surface distortion, it presents no prior defects, thus possessing a perfect fcc core structure.

The most stable surface for Ag is 111, followed by the 100 one,[25] with an energy difference of 6.65%. The third more stable surface, 110, stays above the 111 one with an energy difference of 15.15%, which makes it less likely to occur. Thus, we choose to focus on the 111 and 100 facets and their interactions for the present study.

The effect of temperature in the simulation is important and deserves further commenting. The idea of using high temperatures in MD sintering simulations is attractive to the researcher, since this speeds up the occurrence of processes that could take too long to probabilistically occur at lower temperatures, which helps with the computational costs. However, that practice should include care regarding the fact that nanomaterials behave distinctively from their bulk counterparts, melting effects included.[32] In particular, for Wulff-shaped Ag NPs, the diameter of which is higher than 8 nm, melting simulation involves interactions between quasi-liquid outer atomic layers and the solid NP core.[33] For spherical Ag NPs of 3.0 nm, melting effects in simulations start to show up when close to 600 K[34] and above. Thus, MD simulations of OA phenomena involving NCs at high temperatures[35] are not equivalent to those at lower temperatures, since in the first case the interacting interfaces show liquid-like behavior prior to attachment, while in the latter, solid-like behavior is seen. By performing our simulations at 500 K, we remain, in this work, toward the solid interfaces scenario. Also, special care is necessary when comparing simulations to experiments: for some experiments, such as TEM, the instrument of experimentation affects the solid−liquid behavior of the material being measured. For example, de Knoop et al.[36] melted gold tips at room temperature using only the electron beams of TEM. Our group has used the TEM interactions with materials to induce Ag NP synthesis and coalescence;[8] in that latter case, surface plasmon resonances led to quasi-liquid NP behavior, thus demanding simulations at higher temperatures for proper comparison to experiments. For the present study, proper comparison of simulation to experiments that involve synthesis in colloidal solutions[10,37] is reasonable as long as the temperature in the simulation and in the experiment is chosen in order to have the system in the solid interfaces scenario.

Finally, it is worth mentioning the mechanistic connection between energetics and displacements. Structural changes toward increased thermodynamical stability imply an increase in measured binding energies, which in turn maps to atomic displacements. The opposite, however, can happen but is not always true. (For example, consider the diffusion of a rigid body. The structure does not change and thus, does not the associated binding energy. However, as diffusion evolves, so do the displacements.) In the results section, we chose to display the mean square displacement (MSD) in order to indicate simulation instances at which relevant transitions took place.

https://dx.doi.org/10.1021/acs.jpcc.0c10321
J. Phys. Chem. C 2021, 125, 6812−6820

This choice was made because these signals are strongly related to alignment between NCs. However, it is important to observe that we checked that for each MSD signal there is an equivalent increase in binding energy, as illustrated in the Supporting Information, section S3.

RESULTS AND DISCUSSION

We have chosen a perfect Ag Wulff shaped NC as our archetype of a building block for mesocrystal growth, as illustrated in Figure 1. This NC was chosen with the following considerations in mind: (a) obtain a structure with facets that are large enough to represent stable contact surfaces at the adopted simulation temperature; (b) display exposed crystal facets that are most likely to be found in nature; and (c) avoid a large number of atoms, in order to balance the simulation cost. These considerations are further discussed in the methods section.

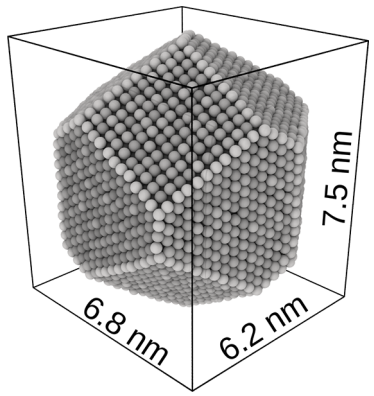

Figure 1. Wulff shaped Ag NC model used in the computational experiments, displaying exposed [100] and [111] crystalline facets.

The procedure illustrated in Figure 2a–h was used to create inputs for the simulations. It starts with cloning the archetype Wulff-shaped Ag NC and translating the copy, so that both NCs face each other with almost touching surfaces (Figures 2a,e). Then, a 40° rotation is applied to one of the NCs in order to have its crystalline plane significantly mismatched relative to the other NC (Figures 2b,f). Then, a displacement $\Delta\vec{r}$ of varying length and direction is applied (Figures 2c,g). Finally, for half the simulations, one last rotation $\Delta\theta = 10°$ is applied (Figures 2d,h), while for the other half, this step is omitted. A total of 160 simulation trials were executed, each taking about a day of supercomputer time to calculate. Half were aimed at studying the interactions between 111 facets and half for the interactions between 100 facets. Events involving complex attachments between more than two facets, as well as mixed 111 and 100 facet interactions, were also observed, since this last case occurs naturally when $\Delta\vec{r}$ becomes large enough.

Attachment between Ag NCs along the 100 facets results in a slow crystallization process, characterized by abrupt transitions between metastable states (for a full picture, check Figures S1 and S2). Each transition quickly leads to a better relative orientation of the NC dimer. To exemplify the relevant transitions and how they contribute to the alignment of the dimer, we show in Figure 3a–g a typical simulation outcome that illustrates the details of the IOA process between 100 interfaces. The first part of the process comprises the initial attachment and formation of a completely amorphous interface between the NCs. This interface will then crystallize under the influence of the two 100 facets that sandwich it. The initial, completely disordered state can last several nanoseconds and, while it lasts, it allows for a smooth, gradual mutual alignment of the NCs through twisting (Figure 3a,b). As crystallization proceeds, eventually the interface evolves from a completely amorphous state into a more ordered one, in which a plastic deformation scenario occurs presenting many unstable dislocations (Figure 3c). From this point on, further order at the interface is attained through the reduction of dislocation nodes (Figures 3d,e). These plastic reconstruction events occur abruptly: when the interface reconstructs itself, decreasing the number of dislocations, a signal is observed in both the mean square displacement (Figure 3) and the average potential energy graphs (Figure S2, top, curve indicated by an orange arrow) and results in an improvement in NC alignment. Eventually, the number of dislocation nodes decreases down to a single one from which four partial Shockley dislocations emerge (Figure 3f), creating a stable plastic deformation at the plane of the interface. These partial Shockley dislocations reduce the energy of the system when compared to perfect dislocations, thus becoming a crystal-

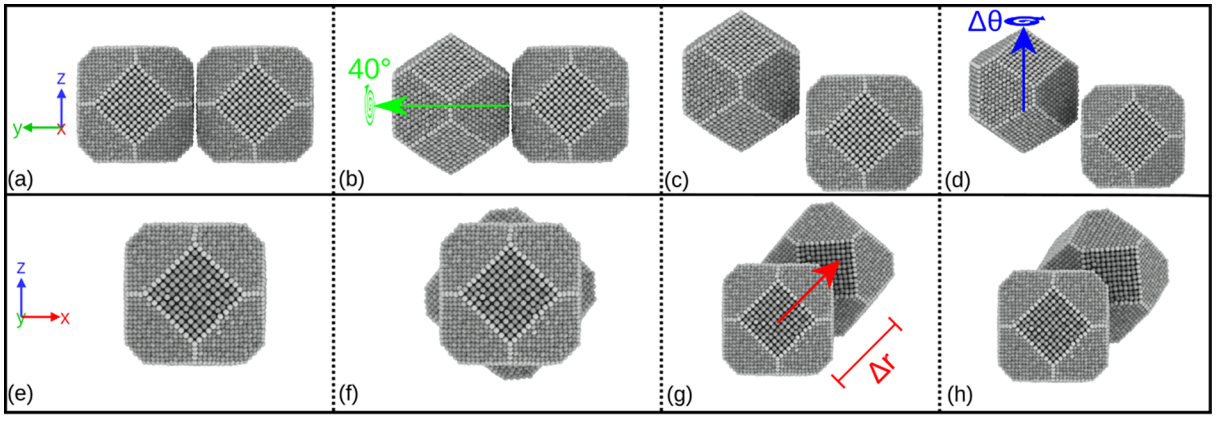

Figure 2. Operations performed to prepare the initial setup for the simulation study. (a) the NC model from Figure 1 is cloned and translated in the $\hat{y}$ direction, forming an almost touching pair. Next, (b) the model on the left is rotated by 40° around the $\hat{y}$ axis. Then, (c) one of the models is dislocated by an amount Δr in the plane spawned by the $\hat{x}$ and $\hat{z}$ vectors. Finally, (d) a $\Delta\theta$ rotation was applied around the $\hat{z}$ axis. Images e, f, g, and h display the same sequence as images a, b, c, and d, respectively, but from a different viewpoint.

https://dx.doi.org/10.1021/acs.jpcc.0c10321
J. Phys. Chem. C 2021, 125, 6812−6820

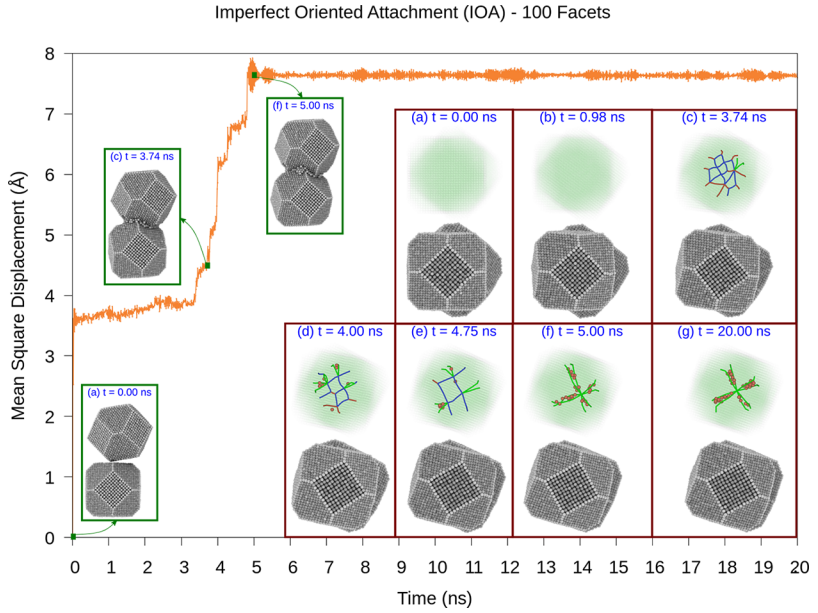

Figure 3. Role of dislocation emergence and evolution during the crystallization process of an Ag NC dimer interface along the 100 facets. In the visualizations, the all atom view is accompanied by a filtered image in which all atoms, except the hcp ones, are made translucent. Blue ribbons indicate perfect, 1/2 ⟨110⟩ dislocations. Green ribbons indicate 1/6 ⟨112⟩ , Shockley partials. Red ribbons indicate unstable dislocations. At 20 ns, one node centered at the middle of the interface from which Shockley partial dislocations emerge in the contact plane spawns four hcp stacking faults that stabilize the structure in a lightly twisted IOA. A video of this example is available in the Supporting Information.

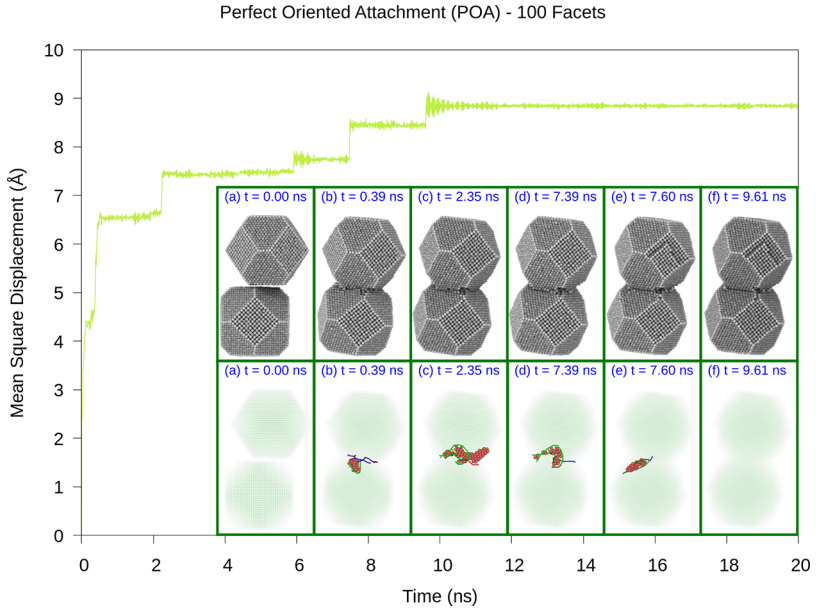

Figure 4. POA process between 100 facets, resulting in a perfectly aligned dimer with a full fcc core structure. The top insets display the complete atomic structure, which in the correspondent bottom insets is shown with a filter that makes amorphous and fcc atoms translucent, leaving visible only dislocations and atoms in a hcp phase. A video of this example is available in the SI.

lization state that is difficult to overcome. This results in an attachment process that ends in IOA, with the dimer presenting a small degree of residual twisting. This outcome was the most common in the simulation batteries involving 100 facets in the conditions set for this study and, thus, is expected to show up in experiments. In fact, in the experiments of Liang et al.[37] the presence of stacking faults was observed in grown Ag nanorice obtained from OA of Ag NCs, a fact that agrees with the predictions obtained in this study. (For a direct comparison, see Figure 3d in their work[37] and compare to Figure 3g in the present study.) These experiments also observed, very clearly, the formation of hcp phases along the direction consistent with OA between 111 facets, which agrees with the simulation results presented herein.

Simulations suggest that POA is an unusual outcome for 100 interacting facets in the conditions chosen for the present study. When it happened, it was triggered by the stabilization of a hcp phase with a component perpendicular to the interface plane during attachment. The existence of such a phase in the interface interferes with the dislocation node dynamics during crystallization, allowing the dimer to skip the formation of the single node stabilized by Shockley partial dislocations (Figure

https://dx.doi.org/10.1021/acs.jpcc.0c10321
J. Phys. Chem. C 2021, 125, 6812−6820

3g) that would lead to IOA. This paves the way for a crystallization route in which unstable hcp stacking faults evolve and heal toward forming a perfect fcc phased dimer, thus removing twisting from the final structure and leading to POA. This behavior, found to be uncommon in the conditions of the present study, was found to be more common in the context of coalescence events between spherical Ag NPs. For a theoretical and experimental analysis of such processes involving spherical Ag NPs, the reader is refered to previous works.[6−8] These results suggest that, by properly exploring the formation of defects that have a component perpendicular to the interface plane during crystallization of 100 facets, one can statistically switch the odds of triggering IOA or POA as desired, thus leading to distinct mesocrystals after self-assembly. One way to induce the formation of such defects, from a simulation perspective, involves attaching the NCs in a specific range of kinetic energies, since attachment impacts with higher kinetic energies lead to the formation of larger defects in such a direction. Another possibility involves exploring quasi-liquid states (the current model presents two of them, adding to the liquid and solid states). From an experimental perspective, this corresponds to keeping the solution in a specific range of temperatures during self-assembly. This analysis suggests that smaller temperatures lead to IOA through the mechanism shown in Figure 3, while slightly larger temperatures (or other defect meddling agent) can trigger the process shown in Figure 4, through the formation of unstable defects during attachment impact. In fact, in the experimental work of Liang et al.,[10] self-assembly of Ag NCs at 100 °C led to the synthesis of Ag nanorice, which presents IOA characteristics when 100 facet interactions are considered, while at higher temperatures, the work led to the synthesis of other structures.

Figure 4 illustrates a POA event between 100 facets, which is an uncommon outcome in the simulation conditions set for this study. The formation of an unstable hcp dislocation (Figure 4b) that grows and shrinks in directions that have a component perpendicular to the plane of the interface prevents the formation of the plastic deformation from Figure 3g, thus providing a crystallization route that ultimately leads to POA. Notice that the evolution of dislocation planes in such a direction leads to the ejection of atoms in one of the noninteracting 100 facets, forming an atomic island there (Figure 4e). Should the temperature be higher (e.g., quasi-liquid state), those atoms could break the energy barrier required in order to migrate from the facet to the interface neck, allowing its thickening and leading to a coalescence process mediated by dislocations that evolve along the neck region, similarly to what was observed by Lange et al.[38] for the case of spherical Au NPs. Each transition in the MSD graph in Figure 4, which also reflects on the average potential energy graph (Figure S1-bottom, indicated by lemon arrow) corresponds to a NC alignment step mediated by interface crystallization.

Opposite to the behavior observed for the 100 facets, attachment between Ag NCs at the 111 facets results in a very fast crystallization process (2 orders of magnitude faster than the process between the 100 facets), in which most of the structures evolved to their final configuration in less than 200 ps (for a full picture, check Figures S3 and S4). Similarly to the observations for 100 facets, attachment between 111 facets usually ends in IOA in the conditions set for the present study, although its final outcome is remarkably different. IOA between 111 facets results in the crystallization of two or more atomic layers of hcp phases, which stabilize the dimer in a twisted shape (see Figure S5 for examples). The effect is mediated by dislocations that evolve the interface from amorphous to plastically deformed during crystallization. In its early stages, the process between 111 facets bears similarities with the one observed for 100 facets, namely the transition from amorphous to plastically deformed with dislocations. Once that occurs, a strikingly different evolution unfolds. To understand it, it is worth mentioning that, for macroscopic fcc solids, dislocating 111 planes can trigger the occurrence of martensitic fcc−hcp transformations, as was observed previously for Al−Ag alloys.[39] Martensitic transformations allow the system to accommodate strain in plastic deformations. In our case, immediately after attachment, the instantaneous situation of the interface is that of an amorphous phase which will try to crystallize following the orientation of the 111 NC facets that sandwich it. This results in severe stress that is capable of twisting the NCs toward mutual alignment. As crystallization proceeds, the number of dislocation nodes is reduced and larger seed domains of the hcp phase develop, leading to a phase transition from fcc to hcp that stabilizes the dimer in IOA, as shown in Figure 6j and Figure S5. Such a situation has a consequence that should be detectable in experiments: when self-assembly occurs with the attachment of many Ag NCs along their 111 direction, thin hcp phases will develop perpendicular to the 111 direction. To see those defects in real experiments, check, for example, Figure 4 in the work of Liang et al.[10]).

On rare occasions, OA between 111 facets which would normally take a few picoseconds of simulation time to occur, can delay for many nanoseconds, in which the system will stay longer in a metastable state. Such uncommon simulation events provide a unique opportunity to glimpse the martensitic transition with further detail. Thus, we choose one of these uncommon events to illustrate the process, which is shown in Figure 6 and Figure S3-bottom (curve indicated by blue arrow). Figure 6 panels b−i detail the crystallization transition from a plastically deformed interface sandwiched between 111 facets containing severe dislocations toward an hcp phase. The martensitic transition acts as nucleating hcp phases that increase in size as the number of dislocation nodes reduce (Figure 6b−e). The process evolves until the system presents a single dislocation node, similarly to what was observed for the interactions between 100 facets. However, differently from what happens at the 100 interfaces, the martensitic transition allows the dissolution of the dislocation nodes through formation of the hcp phase, which quickly grows until the nucleated domains connect, forming a hcp dislocation plane in which the interface stabilizes itself (Figure 6i,j). This difference explains why the OA process between 111 facets is so much quicker than that between 100 facets: the nucleation of the hcp phases greatly accelerates the crystallization process by providing an energetically less expensive pathway for the healing of plastic dislocations.

Being a much faster process, OA between 111 facets makes POA less probable, since NC orientation mediated by crystallization of the interface stops as soon as the formation of the hcp phase ends. Nevertheless, in a few simulation events, the NC alignment process managed to nearly completely align the dimer before stabilization of the hcp phase. These events had in common the fact that they involved the formation of a hcp phase containing a single layer of atoms, as shown in

https://dx.doi.org/10.1021/acs.jpcc.0c10321
J. Phys. Chem. C 2021, 125, 6812−6820

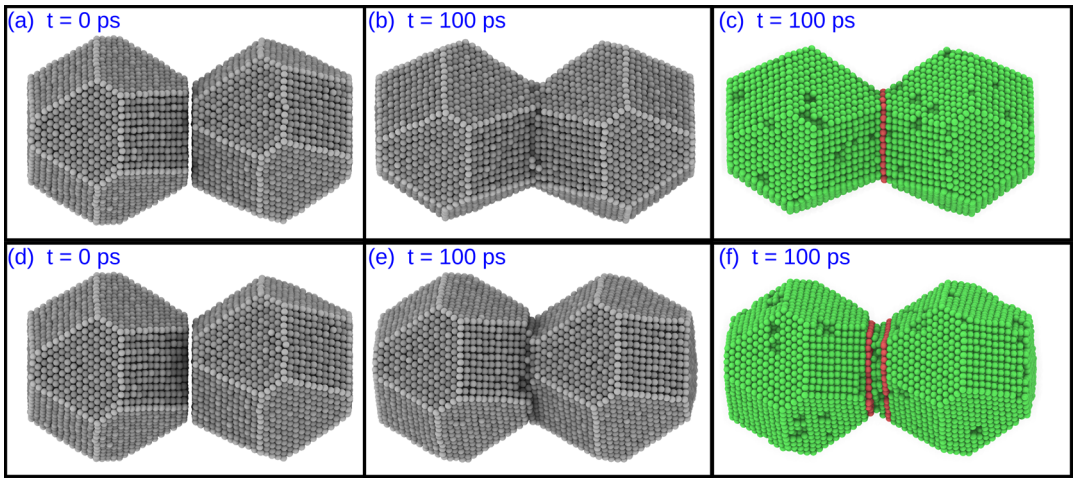

Figure 5. Examples of POA (a–c) and IOA (d–f) events involving 111 Ag NC facets: Panels c and f are, respectively, the same as panels b and e, with the most external layer of atoms made translucent. Green represents a fcc crystal phase and red, a hcp one.

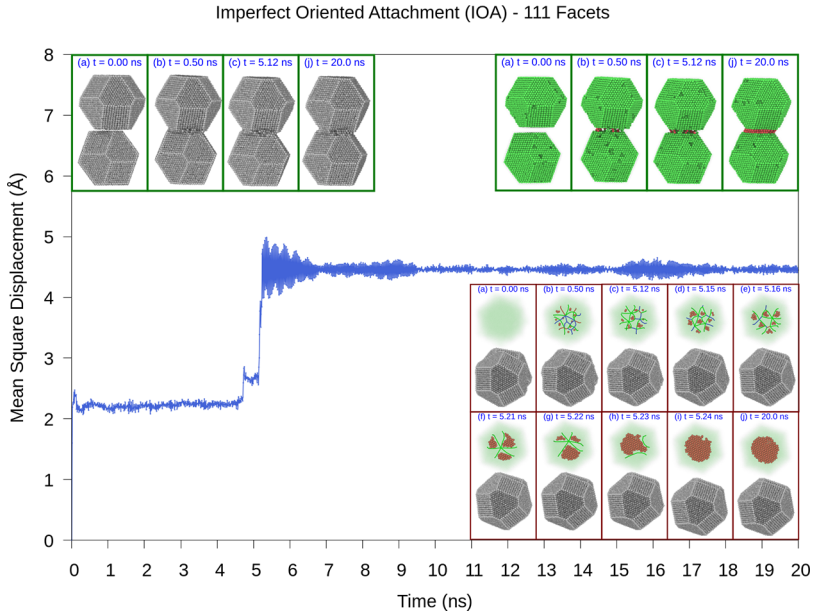

Figure 6. Formation of a hcp phase at the interface between attached 111 facets, in a process in which the system stays for a long period of time in a metastable state between 0.2 to 4.5 ns. Top-left: all-atom view of twisting along the IOA process. Top-right: same as the previous, after applying a filter in which the external layer of atoms is removed, fcc atoms are painted in green and hcp atoms in red, as determined by the CNA analysis method. Bottom-right: Details of the nucleation of an hcp phase mediated by the hcp–fcc martensitic transition. The nucleation involves the formation of an unstable Shockley partial node that quickly degenerates into the hcp phase. A video of this example is available in the Supporting Information.

Figure 5c. On the other hand, IOA typical outcomes involved the transformation of two or more atomic layers of hpc phases, as shown in Figure 5f and Figure S2. These simulation results suggest that POA outcomes between solid 111 facets should be uncommon in experiments, due to the lack of available time for twisting the NCs before stabilization of the interface takes place through its transformation to a hcp phase.

The case for more complex interactions involving mixed 100 and 111 facets has been probed superficially in this work. It occurs naturally, in our simulation method, when Δr is large enough. First of all, the outcomes suggest that, for this situation, simulations longer than 20 ns are required in order to provide time for this more complex scenario to evolve toward its final outcome. Thus, for many trials, at 20 ns most of these simulations did not evolve past the amorphous interface step. For a few cases though, 20 ns was enough to observe the final outcome: either the formation of the hcp phase occurred, when alignment prevailed between 111 facets, or a perfect crystallization of a fcc dimer took place. In these last cases, the multifaceted interaction protects the system from being stuck in the state shown in Figure 3g. Thus, for these multifaceted interactions, the process is more similar to that observed for spherical Ag NPs.[6] Figure 7a–j and Figure S4-bottom (curve indicated by peach arrow) illustrate an example of an attachment event that quickly evolves toward the crystallization of a perfect fcc dimer. Notice that, when facet edges attach, this leads to more significant atomic displacements during the formation of the interface, including the formation of atomic islands over facets. In this interaction, both processes that are characteristic of the 100 facet

https://dx.doi.org/10.1021/acs.jpcc.0c10321
J. Phys. Chem. C 2021, 125, 6812–6820

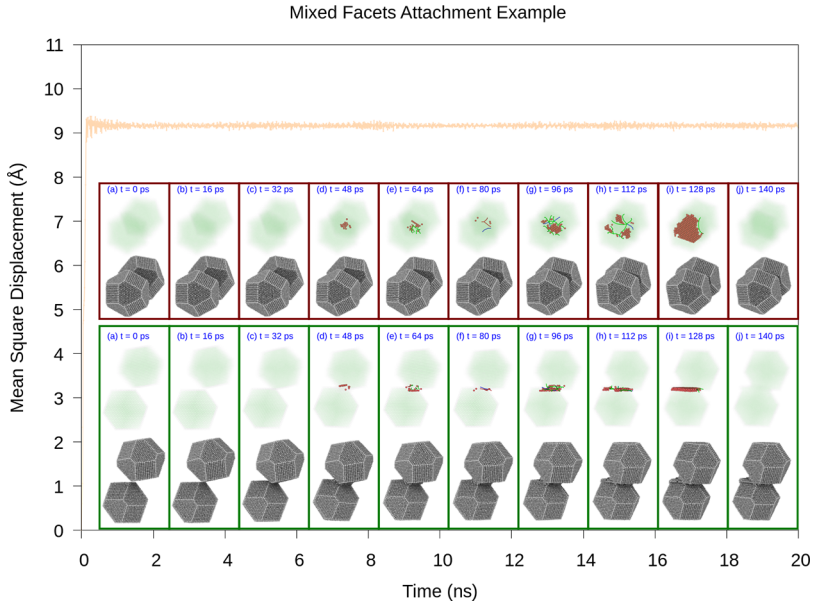

Figure 7. Example of an attachment event in which multiple facets are involved. Notice that the OA process takes only 140 ps to unfold, which is 2 orders of magnitude faster than the process shown in Figure 4. In these more complex events, atomic displacements spawn islands over the exposed facets. The processes previously discussed for 100 and 111 facet interactions both occur, paving the way for healing of the interface into a perfect fcc crystal dimer. A video of this example is available in the SI. Two views of this process are shown.

interaction and the 111 facet interaction take place simultaneously. This helps overcoming energy barriers for the formation of the most stable structure, a POA formation for the fcc dimer. Thus, it indicates that, in experiments, if no control is exerted in order to make attachment more probable between specific facets (e.g., by exploring solvent[13,14] effects), the self-assembly process between Ag NCs leads to the growth of bridged-based mesocrystals that, while interesting in their own right, do not possess the internal crystallization defects shown in the present work that enable the unique technological applications[40] provided by controlled self-assembly when facet selective interactions take place during synthesis.

Finally, it is worth commenting that phenomena in MD simulations evolve in time scales that are faster than those observed in experiments. Processes that in simulations take tenths of ns, in experiments can delay minutes to unfold.[8] Nevertheless, the technique provides good agreement with experiments regarding the structural evolution of the simulated systems, thus being a valid approach to understanding their dynamics.

CONCLUSIONS

- For Ag NCs that are large enough to follow Wulff shapes and remain in the solid state, simulations suggest that the OA process between 100 facets results in a crystallization process that is roughly 2 orders of magnitude slower than its 111 facets counterpart.
- Simulations suggest that OA between 100 facets of Ag NCs leads mostly to IOA, forming a final structure that is twisted. The underlying mechanism is the formation of a defect node stabilized by four Shockley partial dislocations at the plane of the interface. These results appear to agree with published experiments.[37]
- Simulations show that, if the previous mechanism is perturbed through the creation of defects that propagate in a direction that leaves the plane of the interface between the NCs, then the dimer can escape being stuck in IOA and achieves the conditions for POA. Technologies that aim to either achieve POA or IOA between 100 interfaces of Ag NCs should focus in exploring this crystallization mechanism.
- Simulations suggest that IOA is the most common outcome when 111 facets attach. The physical mechanism is distinct and involves the martensitic transformation at the nanoscale. The interface between twisted twinned Ag NCs transforms from amorphous to hcp through the reconstruction of plastic defects during the crystallization process, allowing the self-assembly of complex structures that contain hcp phases. These hcp phases have been observed in published experiments.[10]
- Simulations indicate that POA between 111 facets should be uncommon, as long as they remain in the solid state.
- All the previous results are related to NCs that remain in the solid state. If they reach a quasi-liquid or liquid state, the sintering process turns into coalescence, which leads to distinct outcomes. In particular, in coalescence scenarios (e.g., higher temperatures), the transitions lead to crystallization from amorphous to fcc for Ag NCs, without the formation of permanent hcp phases or defect nodes. This observation agrees with previously published experiments.[10]
- Complex interactions that involve higher values of $\Delta\theta$, thus leading to attachment through corners that contain more than one facet, in general demand simulations longer in time in order to evolve past the amorphous interface step. Occasionally, tough, that can happen through quick transitions that ultimately lead to the formation of a perfect fcc interface. This suggests that, in order to produce new materials that have either the interface defect typical of 100 facet interactions or the hcp phase transformation typical of 111 facet interactions, it is paramount that self-assembly is performed

https://dx.doi.org/10.1021/acs.jpcc.0c10321
J. Phys. Chem. C 2021, 125, 6812−6820

using either surfactants or another control mechanism that works toward minimizing attachment events involving multiple simultaneous facets.

- Last, but not least, it is important to point out that the basic physics of martensitic fcc−hcp transformation, and the one of defect formation in fcc crystals, is not specific of Ag NCs. Although this work focused only in Ag NCs, as did the cited experimental evidence,[10,37,40,41] we believe it is reasonable to speculate that these processes, or at least something similar, should also be observed for materials self-assembled from elementary nanocrystals made of other elements. This speculation is a subject of future research.

■ ASSOCIATED CONTENT

Supporting Information

The Supporting Information is available free of charge at https://pubs.acs.org/doi/10.1021/acs.jpcc.0c10321.

100-100-Interface-IOA-Fig3-article.mp4 (MP4)

00-100-Interface-POA-Fig4-article.mp4 (MP4)

111-111-Interface-IOA-Fig6-article.mp4 (MP4)

111-100-Interface-Mixed-Processes-Fig7-article.mp4 (MP4)

Evolution of the average potential energy as a function of input parameters; defect profiles for 111 facet interaction; comments on OA increase in binding energies; ddditional simulation parameters (PDF)

■ AUTHOR INFORMATION

Corresponding Author

Giovani M. Faccin − *Faculdade de Ciências Exatas e Tecnológicas, Universidade Federal da Grande Dourados-Unidade II, Dourados, Mato Grosso do Sul 79804-970, Brazil; Instituto de Física "Gleb Wataghin", University of Campinas-UNICAMP, Campinas, São Paulo 13083-859, Brazil;* orcid.org/0000-0003-1864-2434; Email: giovanifaccin@ufgd.edu.br

Authors

Zenner S. Pereira − *Departamento de Ciência e Tecnologia, Universidade Federal Rural do Semi-Árido (UFERSA), Campus Caraúbas, Rio Grande do Norte CEP 59780-000, Brazil;* orcid.org/0000-0002-9253-6341

E. Z. da Silva − *Instituto de Física "Gleb Wataghin", University of Campinas-UNICAMP, Campinas, São Paulo 13083-859, Brazil;* orcid.org/0000-0002-2195-0051

Complete contact information is available at: https://pubs.acs.org/10.1021/acs.jpcc.0c10321

Notes

The authors declare no competing financial interest.

■ ACKNOWLEDGMENTS

G. M. Faccin would like to thank IFGW-Unicamp for the institutional support for this work, UFGD for providing a postdoc research program for their teachers and financial support from UFGD through Programa de Apoio à Pesquisa (PAP) - Edital PROPP n° 02/2021. E.Z.D.S. acknowledges support from FAPESP (2013/07296-2, 2016/23891-6 and 2017/26105-4) and CNPq. This work used resources from Centro Nacional de Processamento de Alto Desempenho em São Paulo (CENAPAD-SP), CCJDR IFGW-UNICAMP and SDumont (LNCC), for which the authors are grateful.

■ REFERENCES

(1) Lu, K. Sintering of nanoceramics. *Int. Mater. Rev.* **2008**, *53*, 21−38.

(2) Lee, E. J. H.; Ribeiro, C.; Longo, E.; Leite, E. R. Oriented Attachment: An Effective Mechanism in the Formation of Anisotropic Nanocrystals. *J. Phys. Chem. B* **2005**, *109*, 20842−20846.

(3) Peng, Z.; You, H.; Yang, H. Composition-Dependent Formation of Platinum Silver Nanowires. *ACS Nano* **2010**, *4*, 1501−1510.

(4) Bian, T.; Chu, Z.; Klajn, R. The Many Ways to Assemble Nanoparticles Using Light. *Adv. Mater.* **2020**, *32*, 1905866.

(5) Sahoo, Y.; Cheon, M.; Wang, S.; Luo, H.; Furlani, E. P.; Prasad, P. N. Field-Directed Self-Assembly of Magnetic Nanoparticles. *J. Phys. Chem. B* **2004**, *108*, 3380−3383.

(6) Faccin, G. M.; San-Miguel, M. A.; Andres, J.; Longo, E.; da Silva, E. Z. Computational Modeling for the Ag Nanoparticle Coalescence Process: A Case of Surface Plasmon Resonance. *J. Phys. Chem. C* **2017**, *121*, 7030−7036.

(7) Andrés, J.; Gouveia, A. F.; Gracia, L.; Longo, E.; Manzeppi Faccin, G.; da Silva, E. Z.; Pereira, D. H.; San-Miguel, M. A. Formation of Ag nanoparticles under electron beam irradiation: Atomistic origins from first-principles calculations. *Int. J. Quantum Chem.* **2018**, *118*, No. e25551.

(8) da Silva, E. Z.; Faccin, G. M.; Machado, T. R.; Macedo, N. G.; de Assis, M.; Maya-Johnson, S.; Sczancoski, J. C.; Andrés, J.; Longo, E.; San-Miguel, M. A. Connecting Theory with Experiment to Understand the Sintering Processes of Ag Nanoparticles. *J. Phys. Chem. C* **2019**, *123*, 11310−11318.

(9) Rosenfeld, G.; Morgenstern, K.; Beckmann, I.; Wulfhekel, W.; Lægsgaard, E.; Besenbacher, F.; Comsa, G. Stability of two-dimensional clusters on crystal surfaces: from Ostwald ripening to single-cluster decay. *Surf. Sci.* **1998**, *402−404*, 401−408.

(10) Liang, H.; Zhao, H.; Rossouw, D.; Wang, W.; Xu, H.; Botton, G. A.; Ma, D. Silver Nanorice Structures: Oriented Attachment-Dominated Growth, High Environmental Sensitivity, and Real-Space Visualization of Multipolar Resonances. *Chem. Mater.* **2012**, *24*, 2339−2346.

(11) IMAI, H. Mesocrystals and Their Related Structures as intermediates between single crystals and polycrystals. *J. Ceram. Soc. Jpn.* **2014**, *122*, 737−747.

(12) Bahrig, L.; Hickey, S. G.; Eychmüller, A. Mesocrystalline materials and the involvement of oriented attachment − a review. *CrystEngComm* **2014**, *16*, 9408−9424.

(13) Zhang, H.; De Yoreo, J. J.; Banfield, J. F. A Unified Description of Attachment-Based Crystal Growth. *ACS Nano* **2014**, *8*, 6526−6530.

(14) Balankura, T.; Yan, T.; Jahanmahin, O.; Narukatpichai, J.; Ng, A.; Fichthorn, K. A. Oriented attachment mechanism of triangular Ag nanoplates: a molecular dynamics study. *Nanoscale Adv.* **2020**, *2*, 2265−2270.

(15) Li, D.; Nielsen, M. H.; Lee, J. R. I.; Frandsen, C.; Banfield, J. F.; De Yoreo, J. J. Direction-Specific Interactions Control Crystal Growth by Oriented Attachment. *Science* **2012**, *336*, 1014−1018.

(16) Liu, L.; Nakouzi, E.; Sushko, M. L.; Schenter, G. K.; Mundy, C. J.; Chun, J.; De Yoreo, J. J. Connecting energetics to dynamics in particle growth by oriented attachment using real-time observations. *Nat. Commun.* **2020**, *11*, 1045.

(17) Plimpton, S. Fast Parallel Algorithms for Short-Range Molecular Dynamics. *J. Comput. Phys.* **1995**, *117*, 1−19.

(18) Brown, W. M.; Wang, P.; Plimpton, S. J.; Tharrington, A. N. Implementing molecular dynamics on hybrid high performance computers - short range forces. *Comput. Phys. Commun.* **2011**, *182*, 898−911.

(19) Brown, W. M.; Kohlmeyer, A.; Plimpton, S. J.; Tharrington, A. N. Implementing molecular dynamics on hybrid high performance computers - Particle-particle particle-mesh. *Comput. Phys. Commun.* **2012**, *183*, 449−459.

(20) Brown, W. M.; Yamada, M. Implementing molecular dynamics on hybrid high performance computers-Three-body potentials. *Comput. Phys. Commun.* **2013**, *184*, 2785−2793.
(21) Daw, M. S.; Baskes, M. I. Embedded-atom method: Derivation and application to impurities, surfaces, and other defects in metals. *Phys. Rev. B: Condens. Matter Mater. Phys.* **1984**, *29*, 6443−6453.
(22) Foiles, S. M.; Baskes, M. I.; Daw, M. S. Embedded-atom-method functions for the fcc metals Cu, Ag, Au, Ni, Pd, Pt, and their alloys. *Phys. Rev. B: Condens. Matter Mater. Phys.* **1986**, *33*, 7983−7991.
(23) Johnson, R. A. Alloy models with the embedded-atom method. *Phys. Rev. B: Condens. Matter Mater. Phys.* **1989**, *39*, 12554−12559.
(24) Mishin, Y.; Farkas, D.; Mehl, M. J.; Papaconstantopoulos, D. A. Interatomic potentials for monoatomic metals from experimental data and *ab initio* calculations. *Phys. Rev. B: Condens. Matter Mater. Phys.* **1999**, *59*, 3393−3407.
(25) Sheng, H. W.; Kramer, M. J.; Cadien, A.; Fujita, T.; Chen, M. W. Highly optimized embedded-atom-method potentials for fourteen fcc metals. *Phys. Rev. B: Condens. Matter Mater. Phys.* **2011**, *83*, 134118.
(26) Rassoulinejad-Mousavi, S. M.; Zhang, Y. Interatomic Potentials Transferability for Molecular Simulations: A Comparative Study for Platinum, Gold and Silver. *Sci. Rep.* **2018**, *8*, 2424.
(27) Nosé, S. A molecular dynamics method for simulations in the canonical ensemble. *Mol. Phys.* **1984**, *52*, 255−268.
(28) Nosé, S. A unified formulation of the constant temperature molecular dynamics methods. *J. Chem. Phys.* **1984**, *81*, 511−519.
(29) Hoover, W. G. Canonical dynamics: Equilibrium phase-space distributions. *Phys. Rev. A: At., Mol., Opt. Phys.* **1985**, *31*, 1695−1697.
(30) Honeycutt, J. D.; Andersen, H. C. Molecular dynamics study of melting and freezing of small Lennard-Jones clusters. *J. Phys. Chem.* **1987**, *91*, 4950−4963.
(31) Stukowski, A.; Bulatov, V. V.; Arsenlis, A. Automated identification and indexing of dislocations in crystal interfaces. *Modell. Simul. Mater. Sci. Eng.* **2012**, *20*, 085007.
(32) Sun, J.; He, L.; Lo, Y.-C.; Xu, T.; Bi, H.; Sun, L.; Zhang, Z.; Mao, S. X.; Li, J. Liquid-like pseudoelasticity of sub-10-nm crystalline silver particles. *Nat. Mater.* **2014**, *13*, 1007−1012.
(33) Alarifi, H. A.; Atiş, M.; Özdoğ an, C.; Hu, A.; Yavuz, M.; Zhou, Y. Determination of Complete Melting and Surface Premelting Points of Silver Nanoparticles by Molecular Dynamics Simulation. *J. Phys. Chem. C* **2013**, *117*, 12289−12298.
(34) Wang, X.; Wang, X.; Liu, M.; Wang, Y. Melting suspending of Ag nano-particles monitored by molecular dynamics simulation. *Chem. Phys.* **2019**, *527*, 110459.
(35) Lange, A. P.; Samanta, A.; Olson, T. Y.; Elhadj, S. Quantized Grain Boundary States Promote Nanoparticle Alignment During Imperfect Oriented Attachment. *Small* **2020**, *16*, 2001423.
(36) de Knoop, L.; Juhani Kuisma, M.; Löfgren, J.; Lodewijks, K.; Thuvander, M.; Erhart, P.; Dmitriev, A.; Olsson, E. Electric-field-controlled reversible order-disorder switching of a metal tip surface. *Phys. Rev. Materials* **2018**, *2*, 085006.
(37) Liang, H.; Yang, H.; Wang, W.; Li, J.; Xu, H. High-Yield Uniform Synthesis and Microstructure-Determination of Rice-Shaped Silver Nanocrystals. *J. Am. Chem. Soc.* **2009**, *131*, 6068−6069.
(38) Lange, A.; Samanta, A.; Majidi, H.; Mahajan, S.; Ging, J.; Olson, T.; van Benthem, K.; Elhadj, S. Dislocation mediated alignment during metal nanoparticle coalescence. *Acta Mater.* **2016**, *120*, 364−378.
(39) Furuhara, T.; Maki, T. Accommodation of transformation strain during the growth of precipitates. *Scr. Mater.* **1996**, *34*, 929−934.
(40) Li, M.; Cushing, S. K.; Liang, H.; Suri, S.; Ma, D.; Wu, N. Plasmonic Nanorice Antenna on Triangle Nanoarray for Surface-Enhanced Raman Scattering Detection of Hepatitis B Virus DNA. *Anal. Chem.* **2013**, *85*, 2072−2078.
(41) Shi, H.; Dong, B.; Wang, W. Features of twins and stacking faults in silver nanorice and electron-beam irradiation effect. *Nanoscale* **2012**, *4*, 6389−6392.

https://dx.doi.org/10.1021/acs.jpcc.0c10321
J. Phys. Chem. C 2021, 125, 6812−6820